European Journal of Mechanics B/Fluids 32 (2012) 52–58

Contents lists available at SciVerse ScienceDirect

European Journal of Mechanics B/Fluids

journal homepage: www.elsevier.com/locate/ejmflu

Turbulent velocity measurements in open channel bores

Hubert Chanson *, Nicholas J. Docherty

School of Civil Engineering, The University of Queensland, Brisbane, QLD 4072, Australia

ARTICLE INFO

Article history:
Received 13 December 2010
Received in revised form
18 October 2011
Accepted 20 October 2011
Available online 29 October 2011

Keywords:
Breaking bores
Unsteady turbulent velocity measurements
Acoustic Doppler velocimetry
Ensemble average
Turbulent shear stresses
Tidal bores

ABSTRACT

In an open channel, a sudden rise in free-surface elevation is associated with the development of a bore. The bore front is a hydrodynamic shock with a sharp discontinuity in terms of water depth and velocity field. In this study, some turbulent velocity measurements were conducted in breaking bores. The unsteady turbulent properties were analysed using three methods: an ensemble average (EA) technique based upon 20 repeated experiments, a variable interval time average (VITA) method based upon a single experiment, and the variable interval time average (VITA) method averaged over 20 experimental runs. The instantaneous free-surface and velocity measurements showed a marked effect of the bore front passage. The longitudinal velocity components were always characterised by a rapid flow deceleration at all vertical elevations, and some large fluctuations of all velocity components were recorded beneath the surge. The EA and VITA methods showed some comparable long-term trends superposed to some rapid turbulent fluctuations, as well as close results in terms of the turbulent Reynolds stress components. The VITA data based upon a single run presented some differences with the EA median results, but all methods exhibited comparable long-term trends superposed to rapid turbulent fluctuations.

1. Introduction

A positive surge, also called a hydraulic jump in translation, is generated by the sudden rise in free-surface elevation in an open channel [1–3]. In an estuary with macro-tidal conditions, the rapid water level rise at the river mouth might form such a positive surge, called a tidal bore, during the early flood tide [4–6]. Fig. 1 presents an example of a tidal bore in the Bay of Mont Saint Michel (France). At the bore front, there is discontinuity in terms of the water depth and velocity and pressure fields. The bore is a hydrodynamic shock [7]. Some unsteady velocity measurements, performed using particle image velocimetry and acoustic Doppler velocimetry techniques by Hornung et al. [8] and Koch and Chanson [9] highlighted some large velocity fluctuations during the bore passage.

Field measurements in tidal bores are rare, despite their relevance. Several studies experienced some damage to the scientific equipment, including in the Rio Mearim (Brazil), in the Daly River (Australia), in the River Dee (UK), and in the Sélune River (France) [10–13]. The field works further showed some massive sedimentary processes in Alaska, China, and France [14–16]. For example, the author saw the Sélune River in the Bay of Mont Saint Michel (Fig. 1) cutting a new river channel during a single flood tide event on 31 August 2008, and other channel incision events were observed (Tessier 2008, Person. Comm.). In the natural system, the channel bathymetry does change rapidly and it is a challenge to characterise the flow turbulence based upon a unique experimental data set.

In this study, the turbulence properties of bores in open channels were investigated physically under controlled flow conditions. The free-surface fluctuations and turbulent velocity components were measured simultaneously, and the experiments were repeated 20 times with two different configurations. The turbulence properties of the breaking bore were analysed using three methods. The results were compared and discussed in the context of a hydrodynamic shock propagating in an open channel.

2. Experimental apparatus and procedures

The experiments were performed in a 12 m long, 0.5 m wide tilting flume (Fig. 2). The channel was made of a smooth PVC bed and glass walls, and the water was supplied by a constant head tank. A fast-closing gate was located next to the channel downstream end ($x = 11.15$ m), where x is the distance from the channel upstream end. The experiments were performed with two types of bed roughness (Table 1). Some experiments were performed with the smooth PVC bed. For other experiments, the invert was covered with a series of plywood sheets covered by natural blue granite gravels which were sieved between 4.75 and 6.70 mm, glued in resin, and covered by a spray gloss surface

* Corresponding author. Tel.: +61 7 33653516; fax: +61 7 33 65 45 99.
E-mail address: h.chanson@uq.edu.au (H. Chanson).

0997-7546/$ – see front matter © 2011 Elsevier Masson SAS. All rights reserved.
doi:10.1016/j.euromechflu.2011.10.001

Table 1
Experimental studies of unsteady turbulence in tidal bores.

Reference (1)	Q (m^3/s) (2)	B (m) (3)	S_o (4)	d_o (m) (5)	V_o (m/s) (6)	δ/d_o (7)	Fr (8)	Bed roughness (9)
[8]	0	–	0	–	0	N/A	1.5–6	Smooth bed
[9]	0.040	0.50	0	0.079	1.01	0.61	1.31–1.93	Smooth PVC
Present study								
Series 1	0.050	0.50	0	0.118	0.85	0.475	1.08–1.59	Smooth PVC
			0.002	$0.125^{(+)}$	0.80	0.64	1.01–1.52	Fixed gravel bed ($k_s = 3.4$ mm)
Series 2	0.050	0.50	0.000	0.117	0.85	0.475	1.61	Smooth PVC
(ADV measurements)			0.002	0.126	0.79	0.64	1.50	Fixed gravel bed ($k_s = 3.4$ mm)

Notes: B: channel width; d_o: initial water depth at $x = 5$ m; Fr: tidal bore Froude number; k_s: equivalent sand roughness height; Q: initial flow rate; S_o: bed slope; V_o: initial flow velocity at $x = 5$m; $^{(+)}$: measured above the roughness.

Fig. 1. Breaking tidal bore of the Sélune River in the Bay of Mont Saint Michel on 24 September 2010. Bore propagation from right to left. Flow conditions: $d_o = 0.37$ m, $U = 2$ m/s, $(V_o + U)/\sqrt{g\ d_o} = 1.5$.

finish (Fig. 2B). The hydraulic roughness of the fixed gravel bed was tested for a range of steady flow conditions; the equivalent Darcy–Weisbach friction factor f of the fixed gravel bed ranged from 0.031 to 0.045. The results were basically independent of Reynolds number and relative roughness, yielding on average $f = 0.036$, which corresponded to an equivalent sand roughness height $k_s = 3.4$ mm, which was comparable to the typical gravel size $d_s = 5.7$ mm.

The steady flow rate was measured with two orifice meters that were calibrated on site with a volume per time technique. The percentage of error was expected to be less than 2%. In steady flows, the water depths were measured using rail-mounted pointer gauges. The unsteady water depths were recorded using several acoustic displacement meters, Microsonic™ Mic + 25/IU/TC, with a response time of less than 50 ms and an accuracy of 0.2 mm. The acoustic displacement meters were calibrated against the pointer gauges in steady flows.

The turbulent velocity measurements were performed with an acoustic Doppler velocimeter (ADV), Nortek™ Vectrino + (Serial No. VNO 0436), equipped with a side-looking head (Fig. 2B). The velocimeter head is seen above the free surface in Fig. 2B. During the experiments, the velocity range was 1.0 m/s, and the data accuracy was 0.01 m/s. The translation of the ADV probe in the vertical direction was controlled by a fine adjustment travelling mechanism connected to a Mitutoyo™ digimatic scale unit. The error on the vertical position of the probe was $\Delta z < 0.025$ mm, where z is the vertical elevation. The accuracy on the longitudinal position was estimated as $\Delta x < +/- 2$ mm. The accuracy on the transverse position of the probe was less than 1 mm. Herein all the measurements were taken on the channel centreline, since some earlier works showed little transverse differences, but close to the sidewall where the acoustic Doppler velocimetry could be adversely affected by the sidewall proximity [17,9].

Further information on the experimental apparatus was reported by Docherty and Chanson [18].

2.1. Acoustic Doppler velocimetry data post-processing

During some initial tests, the ADV signal outputs contained numerous errors, associated with low correlations and low signal to noise ratios, caused by some inadequate seeding of the tap water. Thereafter, the channel was seeded with about 100 g of Clay Ceram for every hour of channel operation. The clay powder was introduced in the intake structure upstream of the channel test section and dispersed progressively with time. All reported experimental data were conducted with some seeding.

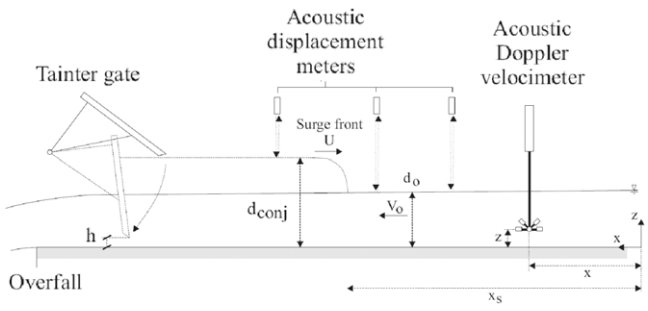

(A) Definition sketch.

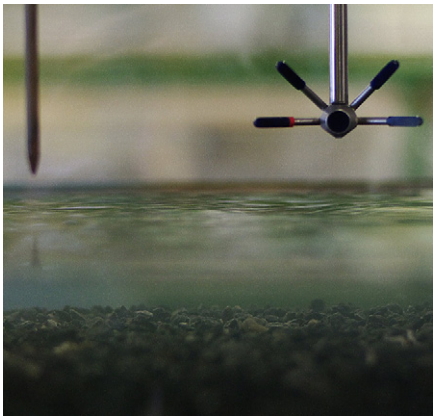

(B) Photograph of the flume with the gravel bed configuration, and the pointer gauge (left) and ADV head (right) above the free surface.

Fig. 2. Experimental channel.

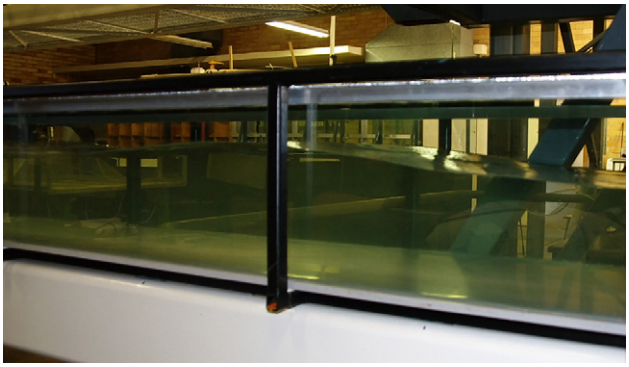

(A) Undular bore propagating from left to right. $Q = 0.050$ m^3/s, $d_o = 0.139$ m, Fr ≈ 1.1, $h = 0.050$ m, shutter speed 1/50 s. The wave crest was at about $x = 1$ m.

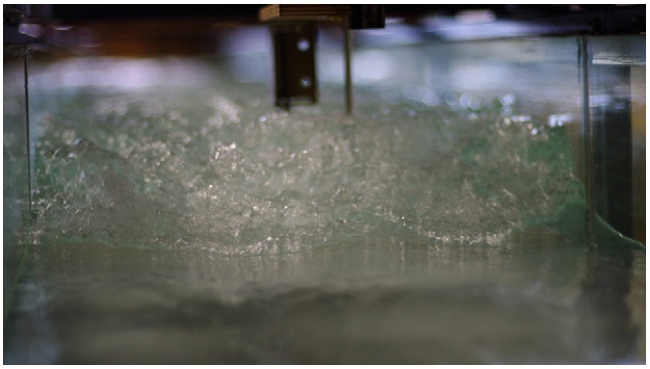

(B) Looking downstream at the incoming breaking bore roller. $Q = 0.050$ m^3/s, $d_o = 0.116$ m, $U = 0.85$ m/s, Fr $= 1.6$, smooth PDV bed, high-speed photograph (shutter speed 1/100 s).

Fig. 3. Photographs of positive surges and bores.

The post processing of ADV data was conducted using a similar method to that of [9]. To characterise the steady flow properties only, the ADV post-processing included the removal of communication errors, the removal of average signal to noise ratio data less than 5 dB, the removal of average correlation values less than 60%, and the application of the phase-space thresholding technique to remove spurious spikes from the data set [19]. The percentage of erroneous data was less than 15% in steady flows, but close to the bed ($z < 0.030$ m) where the percentage was less than 30%.

In unsteady flow conditions, the above post-processing technique was not applicable (Nikora 2004, Person. Comm., [9]). The unsteady flow post-processing was limited to a removal of communication errors, and it is acknowledged that the vertical velocity component V_z data might be affected adversely by the bed proximity for $z < 0.030$ m.

2.2. Experimental flow conditions and bore generation

The experimental setup was selected to generate a range of bores with the same initial flow rate Q (Table 1). The dependent parameters were the bed roughness and the downstream gate opening after closure h. For each experimental run, the steady gradually varied flow conditions were established for 5 min prior to the measurement start. The tidal bore was generated by the rapid partial closure of the downstream gate (Fig. 2A). The gate closure time was less than 0.15 s. After closure, the bore propagated upstream (Fig. 3), and each experiment was stopped before the bore front reached the channel upstream end. The initial flow conditions as well as the tidal bore generation were highly repeatable.

Two series of experiments were conducted (Table 1). The first series focused on the general flow patterns and free-surface properties recorded between $x = 4$ and 6 m. In the second series of experiments, some detailed velocity measurements were conducted at $x = 5$ m, and the ADV and displacement sensors were sampled simultaneously at 200 Hz and synchronised within 5 ms. The velocity measurements were performed with flow conditions that could be considered roughly as a 3:1 scale study of the breaking bore seen in Fig. 1.

Some preliminary steady flow measurements showed that, at $x = 5$ m, the velocity profile was partially developed. The relative boundary layer thickness δ/d_o was 0.47 and 0.64 for the smooth PVC bed and fixed gravel bed, respectively, where δ is the boundary layer thickness and d_o is the initial flow depth at $x = 5$ m (Table 1, column 7).

2.3. Turbulent velocity calculations

In a turbulent flow, the instantaneous velocity V is typically decomposed into an average component $\overline{V}$ and a turbulent fluctuation v: $V = \overline{V} + v$. In a steady turbulent flow, $\overline{V}$ is the time average. In an unsteady flow, the long-term trend and the short-term turbulent fluctuations must be processed separately [20,21]. A technique consists in the repetition of the same experiment N times, and $\overline{V}$ is the ensemble average [20,22]. Other techniques may be based upon the phase-averaging method of periodic flows [23], or some decomposition of turbulent time or length scales [24,25]. Another technique separates the distinctive long-term trend from the short-term fluctuation frequencies, and the variable interval time average (VITA) $\overline{V}$ is a low-pass filtered component [21].

In the present study, a series of 20 instantaneous velocity records was repeated at three vertical elevations ($z/d_o = 0.135$, 0.434, and 0.733) in a manner such that the initial flow conditions were perfectly identical for each run, where z is the vertical elevation and d_o the initial flow depth. An ensemble median of each instantaneous velocity component was produced for each vertical elevation. Similarly, the variable interval time average (VITA) was calculated for each run. The VITA decomposition was based upon a band pass filter, with a cut-off frequency $F_{cutoff} = 2$ Hz derived from a sensitivity analysis [18].

The overall results were used to compare the ensemble median of the 20 runs, the median VITA value of the same 20 runs, and the VITA value of a single run (Table 2). The first two methods can only be applied to laboratory experiments performed under controlled flow conditions, while the third method might be applicable to field measurements [26,13].

3. Basic observations

3.1. Presentation

Some visual observations were conducted for a range of flow conditions listed in Table 1. Several patterns were observed to be functions of the bore Froude number, defined as

$$\text{Fr} = \frac{V_o + U}{\sqrt{g\ d_o}} \quad (1)$$

where V_o is the initial flow velocity positive downstream, g is acceleration due to gravity, and U is the surge front celerity positiveupstream (Fig. 2A). The Froude number is defined herein in the system of coordinates in translation with the surge [7,2]. For a

Table 2
Turbulent velocity processing techniques (used in the present study).

Processing technique (1)	Number of experiments (2)	Basic processing (3)	Application (4)
Ensemble average (EA) median	20 repeats	Ensemble median	Laboratory
Variable interval time average (VITA)	20 repeats	Filtering + ensemble median	Laboratory
Variable interval time average (VITA)	1 run	Filtering	Field data

Froude number between unity and 1.5, the tidal bore was undular. That is, the tidal bore front was followed by a train of secondary quasi-periodic waves called undulations (Fig. 3A). For larger Froude numbers (Fr > 1.5–1.6), a breaking bore was observed (Figs. 1 and 3B). It was characterised by a marked turbulent roller.

The undular bore had a smooth, quasi-two-dimensional free-surface profile for Fr < 1.2 for smooth PVC and Fr < 1.4 for rough gravel bed respectively (Fig. 3A). For 1.2–1.4 < Fr, some slight cross-waves (or shock waves) were observed, starting next to the sidewalls upstream of the first wave crest and intersecting next to the first crest on the channel centreline. For 1.3–1.45 < Fr < 1.5, some slight breaking appeared at the first wave crest next to the channel centreline, and the secondary waves became flatter. The size and strength of the roller increased with increasing Froude number until the roller occupied the entire channel width. At the largest bore Froude numbers (i.e., Fr > 1.5), the surge had a marked roller, and appeared to be quasi-two-dimensional (Fig. 3B). There was no shock wave and the free surface behind the roller was approximately horizontal, although some large free-surface fluctuations were observed. Some air entrainment and intense turbulent mixing were seen in the bore roller.

Overall, the present findings were comparable to earlier observations [27,28,8,9]. In particular, the tidal bore flow patterns were independent of the bed roughness.

3.2. Ratio of conjugate depths

In a bore, the flow properties immediately upstream and downstream of the front must satisfy the continuity and momentum principles [1,2]. Considering a bore travelling in a horizontal rectangular channel, the integral form of the equations of conservation of mass and momentum gives a series of relationships between the flow properties in front of and behind the bore front:

$$\frac{d_{conj}}{d_o} = \frac{1}{2}\left(\sqrt{1+8\,\mathrm{Fr}^2}-1\right), \quad (2)$$

where d is the water depth, the subscript o refers to the initial flow conditions and the subscript $conj$ refers to the conjugate flow conditions, or new flow conditions, immediately after the bore passage (Fig. 2A). Eq. (2) gives an expression of the ratio of conjugate depths as a function of the bore Froude number, and it is based the assumption of hydrostatic pressure distribution in front of and behind the bore front, while the friction losses are neglected.

For the present experiments, the data for the conjugate depth ratio d_{conj}/d_o are presented in Fig. 4 and compared with those from Eq. (2) and some prototype and laboratory data. The results highlighted a reasonable agreement between data and theory for both the smooth and rough bed configurations. The finding was consistent with a number of earlier observations [1,29].

3.3. Instantaneous free-surface and velocity measurements

During the second series of experiments (Table 1), the free-surface and velocity components were sampled simultaneously on the channel centreline at $x = 5$ m, with the ADV sampling volume elevation in the range $0.0058 < z < 0.09$ m. On the fixed gravel bed, the vertical elevation z was measured above the top of the

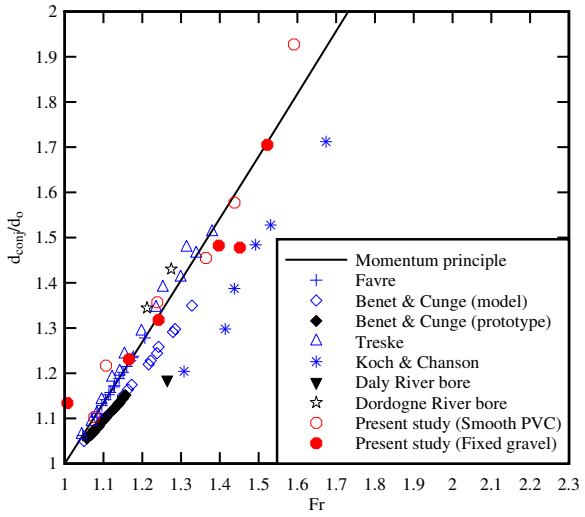

Fig. 4. Ratio of conjugate depths d_{conj}/d_o as a function of the bore Froude number. Comparison between the present data (red symbols), earlier laboratory studies (blue symbols: [27,30,28,9]), prototype data (black symbols: [30], [31] [Dordogne River], [11] [Daly River]), and the momentum equation (Eq. (2)). (For interpretation of the references to colour in this figure legend, the reader is referred to the web version of this article.)

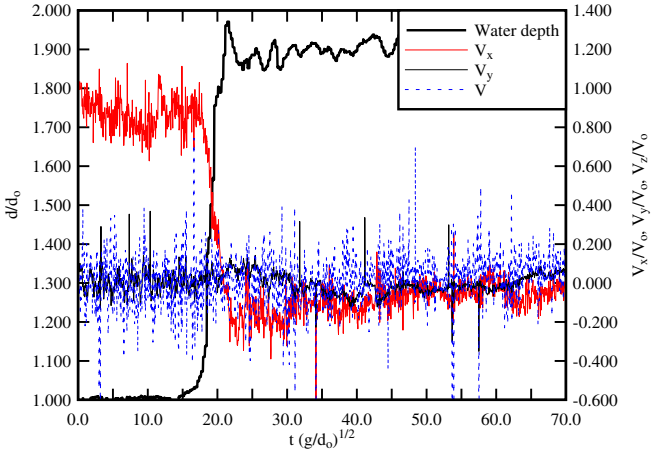

Fig. 5. Instantaneous free-surface elevation and turbulent velocities in a breaking bore on smooth PVC bed. $Q = 0.050$ m^3/s, $d_o = 0.117$ m, Fr = 1.6, ADV sampling volume elevation $z/d_o = 0.091$.

gravel bed using a semi-circular footing with a 25.1 cm^2 area. Fig. 5 illustrates a typical data set in the form of the dimensionless time variations of instantaneous free-surface elevation and velocity components. Herein the instantaneous velocity components V_x, V_y, and V_z were positive downstream, towards the left sidewall, and upwards, respectively.

On the smooth PVC bed, the surge was a breaking bore without residual free-surface undulations (Fig. 5). On the rough gravel bed, the surge had a marked roller followed by some small residual undulations, possibly linked with a small difference in bore Froude number. Both the free-surface data and the visual observations showed that the free-surface elevation rose first

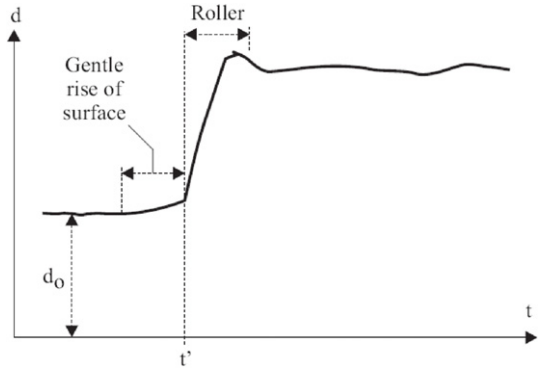

Fig. 6. Sketch of the instantaneous free-surface measurement data during the breaking bore front passage.

slowly, immediately prior to the roller (Figs. 5 and 6). Such gradual rise in free surface ahead of the turbulent roller is sketched in Fig. 6 and was previously reported by Hornung et al. [8] and Koch and Chanson [9]. In Fig. 6, the characteristic time t' corresponded to the free-surface discontinuity between the gentle free-surface rise and the turbulent roller. For $t > t'$, the turbulent roller caused a sharp rise in the water elevation seen in Figs. 3B and 5.

For both smooth and fixed gravel bed configurations, the longitudinal velocity data highlighted a rapid deceleration during the passage of the bore roller. As the bore front reached the sampling volume ($x = 5$ m), the water depth increased first gradually with time for $t < t'$ (Fig. 5). The gradual rise in free surface was associated with a gradual longitudinal deceleration, and was followed by a sudden increase in the free-surface elevation during the roller passage ($t > t'$). The sudden rise in water depth was associated with a sharp decrease in longitudinal velocity component, seen in Fig. 5. Further, some transient negative longitudinal velocities V_x were observed next to the invert (Fig. 5). This transient recirculation pattern was observed for $z/d_o < 0.31$ on the smooth PVC bed and $z/d_o < 0.56$ on the fixed gravel bed. Above, the longitudinal velocity component tended to remain positive for the entire bore passage record. The observations implied the existence of an unsteady recirculation pattern that was associated with some large turbulent stresses in the water column and would induce some major impact in a natural system in terms of sediment processes and particulate dispersion.

Most characteristic features were similar for both the smooth PVC and fixed gravel beds, although the bed roughness had a noticeable effect on the recirculation patterns in the flow.

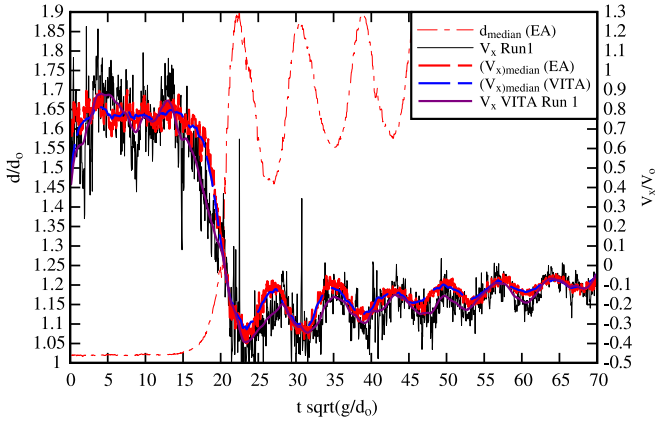

Fig. 8. Dimensionless ensemble-averaged median water depth d_{median} (thin red line), ensemble-averaged median longitudinal velocity component V_{median} (thick red dashed line), instantaneous data (Run 1, thin black line) and the low-pass filtered velocity component (VITA, Run 1) (thick purple dashed line). Fixed gravel bed, $Q = 0.050$ m^3/s, $d_o = 0.126$ m, Fr $= 1.5$, ADV sampling volume elevation $z/d_o = 0.131$. (For interpretation of the references to colour in this figure legend, the reader is referred to the web version of this article.)

4. Unsteady turbulence properties

4.1. Presentation

A series of 20 instantaneous free-surface and velocity measurements was repeated, and the data were synchronised in terms of the characteristic time t' (Fig. 6). Both the ensemble average (EA) and variable interval time average (VITA) techniques were applied. Fig. 7 illustrates some typical difference in signal processing techniques. Fig. 7 presents the median water depth d_{median} and median velocity component $(V_x)_{median}$, both as an EA over the 20 runs, the low-pass filtered velocity component, and as a VITA, of each run, and the median VITA value for the 20 runs. Fig. 7A shows some longitudinal velocity data and Fig. 7 some vertical velocity data. Fig. 8 presents a further comparison between a longitudinal data set (Run 1), the VITA of the single run, and the median velocity component $(V_x)_{median}$. Some preliminary remarks may be derived from Figs. 7 and 8. The median VITA value for the 20 runs and the ensemble-averaged median data yielded close results in terms of all turbulent velocity components (Fig. 7). The VITA data based upon a single run provided the general trends despite some difference with the EA results (Fig. 8).

Overall, both the EA and VITA data showed some seminal features of the breaking bores: (a) a rapid flow deceleration during

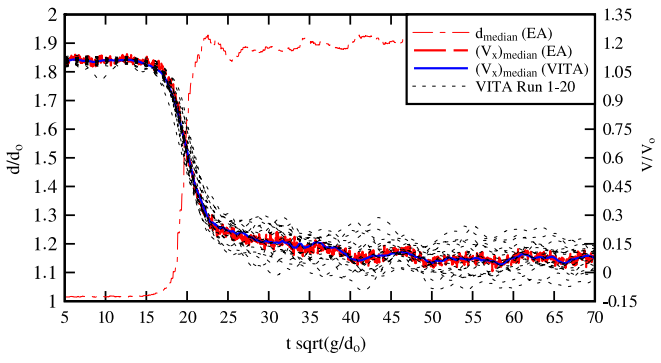

(A) Longitudinal velocity component V_x.

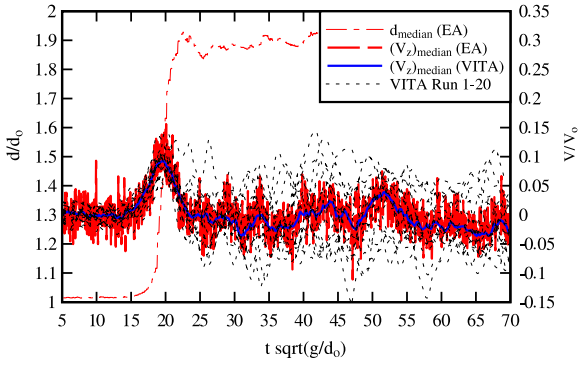

(B) Vertical velocity component V_z.

Fig. 7. Dimensionless ensemble-averaged median water depth d_{median}, ensemble-averaged median velocity component V_{median} (thick red dashed line), median value of the variable interval time average (VITA) velocity component (median value of 20 runs) (thick blue solid line), and low-pass filtered velocity components (VITA, Runs 1–20) (thin black dotted lines). Smooth PVC bed, $Q = 0.050$ m^3/s, $d_o = 0.117$ m, Fr $= 1.6$, ADV sampling volume elevation $z/d_o = 0.434$. (For interpretation of the references to colour in this figure legend, the reader is referred to the web version of this article.)

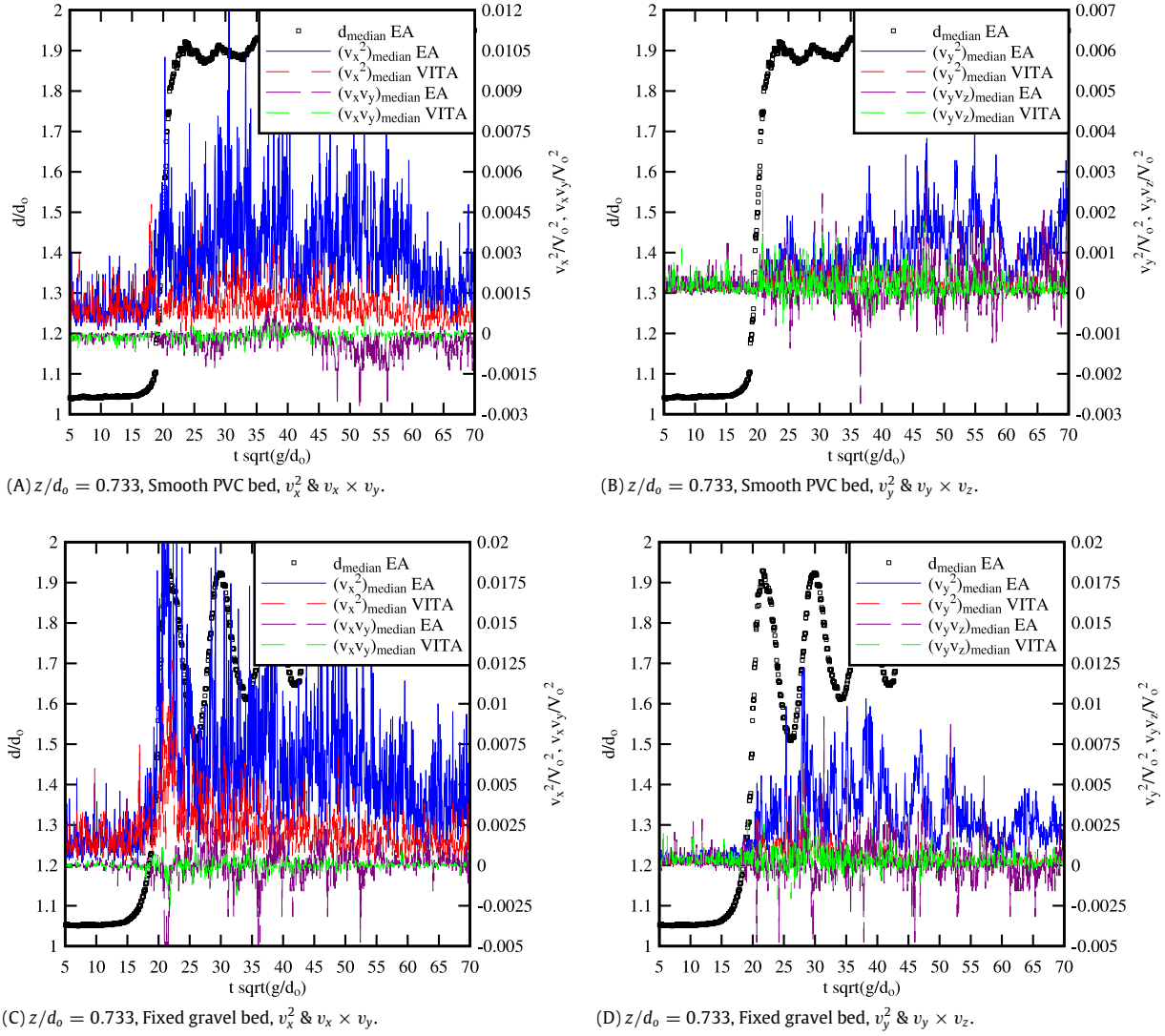

Fig. 9. Dimensionless ensemble-averaged median water depth d_{median}/d_o and median Reynolds stresses v_x^2/V_o^2 and $v_x \times v_y/V_o^2$ (left), and v_y^2/V_o^2 and $v_y \times v_z/V_o^2$ (right) on smooth PVC and fixed gravel beds. Comparison between EA and VITA calculations.

the passage of the tidal bore roller above the sampling volume, (b) some negative longitudinal velocity component next to the bed, highlighting some transient recirculation "bubble", and (c) some positive vertical velocity component beneath the roller. The latter was believed to be closely linked with the streamline curvature immediately prior to the bore roller ($t < t'$) and possibly during the roller propagation ($t' < t$). The experimental results showed further that the passage of the roller was always associated in some large free-surface fluctuations, associated with some large velocity fluctuations and some transient upward flow motion ($V_z > 0$).

The experimental results indicated that the EA median data were very close to the median VITA value for the 20 runs (Figs. 7 and 8). The finding was interesting practically since the ensemble-averaging method required less processing. The results highlighted however some differences: the time variations of the VITA data for each individual run presented some scatter compared to the ensemble-averaged median value (Figs. 7 and 8). However, all the techniques provided some comparable long-term trends superposed to rapid turbulent fluctuations of the turbulent velocity components. Lastly note the scatter of the ensemble-averaged data around the long-term tend. It is acknowledged that the number of experimental repeats (20 herein) was small.

4.2. Turbulent Reynolds stresses in breaking tidal bores

The Reynolds stress tensor is a transport effect resulting from turbulent motion induced by velocity fluctuations with its subsequent increase of momentum exchange and of mixing. Herein the instantaneous turbulent stresses were calculated using the EA and VITA techniques for the experimental flow conditions summarised in Table 1. Some typical results are presented in Fig. 9. In Fig. 9, the median Reynolds stress tensor components were calculated using either the EA method or the VITA method (median value of 20 runs).

The turbulent stress results showed a number of interesting features. The Reynolds stress data suggested that the passage of breaking tidal bores was associated with large and rapid fluctuations of all the turbulent stresses at all vertical elevations. That is, the magnitude of the Reynolds stress tensor components was significantly larger than prior to the bore passage. For example, on the smooth PVC bed (Fig. 9A), the normal stress $\rho \times v_x^2$ increased from 0.6 Pa on average prior to the bore to 2.5 Pa on average beneath the breaking bore; similarly, on fixed gravel bed (Fig. 9C), $\rho \times v_x^2$ increased from 0.8 Pa on average prior to the bore to 4 Pa on average below the bore. The findings were observed for all Reynolds stress components. The result was consistent with the

observations of [9], but that study deduced the turbulent stresses from a VITA analysis performed on a single experiment. Koch and Chanson did not present any ensemble-averaged or VITA median data.

Further, the three processing techniques yielded similar results in terms of the Reynolds stresses. For example, both the ensemble-averaging and variable interval time averaging techniques yielded comparable results in terms of v_x^2 and $v_x v_y$ (Fig. 9).

5. Conclusion

In a highly unsteady flow, such as a shock, the turbulence measurements technique must be adapted, and this is detailed herein for positive surges and bores in an open channel. The experimental results demonstrated that the propagation of a breaking bore induced some substantial turbulent mixing. The passage of the bore front was associated with some large water depth fluctuations. Both the instantaneous and ensemble-averaged turbulent velocity data highlighted some basic features of the flow field in tidal bores. Namely, a strong flow deceleration was observed at all elevations during the breaking bore passage. Close to the bed, the longitudinal velocity component became negative immediately after the roller passage, implying the existence of a transient recirculation "bubble". The height and duration of the transient was a function of the bed roughness, with a longer higher recirculation region above the fixed gravel bed. The vertical velocity data presented some positive upward motion during the bore passage with increasing maximum vertical velocity with increasing distance from the bed, and it was believed to be linked with some streamline curvature. The transverse velocity data presented some large fluctuations with non-zero ensemble average after the roller passage that highlighted some intense secondary motion advected behind the bore front.

A comparison between three processing techniques was developed (Table 2). The experimental findings highlighted a number of key features.

(a) Both the ensemble average (EA) performed over 20 runs and the ensemble median of 20 variable interval time averages showed some comparable long-term trends superposed to some rapid turbulent fluctuations. The result is valuable indicating that the method with the least processing (EA technique) was suitable in a laboratory under controlled flow conditions.

(b) The VITA data based upon a single run presented some differences with the EA median results in terms of all velocity components.

(c) The turbulent stress data showed comparable results with both EA and VITA techniques. The passage of the breaking bore was associated with large and rapid fluctuations of all turbulent stress components at each vertical elevation.

(d) All the techniques provided some comparable long-term trends superposed to rapid turbulent fluctuations of the turbulent velocity components.

Overall, the study highlighted the intense turbulence and turbulent mixing during the passage of breaking bores and surges in open channels. The findings suggested further that the VITA method for a single run gave the general trends and basic flow features; hence it may be a suitable technique for field measurements in tidal bores propagating in natural channels with movable boundaries and changing bathymetry between tides.

Acknowledgements

The authors acknowledge the technical assistance of Graham Illidge and Clive Booth (The University of Queensland). The authors also thank Prof. Laurent David (University of Poitiers, France), Dr. David Reungoat (University of Bordeaux, France), and Prof. C.J. Apelt (University of Queensland, Australia) for their helpful advice.

References

[1] F.M. Henderson, Open Channel Flow, MacMillan Company, New York, USA, 1966.
[2] J.A. Liggett, Fluid Mechanics, McGraw-Hill, New York, USA, 1994.
[3] H. Chanson, Current knowledge in hydraulic jumps and related phenomena, a survey of experimental results, Eur. J. Mech. B. Fluids 28 (2) (2009) 191–210. doi:10.1016/j.euromechflu.2008.06.004.
[4] Rayleigh, Lord, Note on tidal bores, Proc. R. Soc. Lond. 81 (541) (1908) 448–449. Series A Containing Papers of a Mathematical and Physical Character.
[5] D.H. Peregrine, Calculations of the development of an undular bore, J. Fluid Mech. 25 (1966) 321–330.
[6] H. Chanson, Current knowledge in tidal bores and their environmental, ecological and cultural impacts, Enviro. Fluid Mech. 11 (1) (2011) 77–98. doi:10.1007/s10652-009-9160-5.
[7] J. Lighthill, Waves in Fluids, Cambridge University Press, Cambridge, UK, 1978, p. 504.
[8] H.G. Hornung, C. Willert, S. Turner, The flow field downstream of a hydraulic jump, J. Fluid Mech. 287 (1995) 299–316.
[9] C. Koch, H. Chanson, Turbulence measurements in positive surges and bores, J. Hydraul. Res. IAHR 47 (1) (2009) 29–40. doi:10.3826/jhr.2009.2954.
[10] B. Kjerfve, H.O. Ferreira, Tidal bores: first ever measurements, Ciência e Cultura J. Brazilian Assoc. Adv. Sci. 45 (2) (1993) 135–138.
[11] E. Wolanski, D. Williams, S. Spagnol, H. Chanson, Undular tidal bore dynamics in the Daly Estuary, Northern Australia, Estuarine Coastal Shelf Sci. 60 (4) (2004) 629–636. doi:10.1016/j.ecss.2004.03.001.
[12] J.H. Simpson, N.R. Fisher, P. Wiles, Reynolds stress and TKE production in an estuary with a tidal bore, Estuarine Coastal Shelf Sci. 60 (4) (2004) 619–627.
[13] D. Mouze, H. Chanson, B. Simon, 2010 Field measurements in the tidal bore of the Sélune river in the Bay of Mont Saint Michel, September 2010, Hydraulic Model Report No. CH81/10, School of Civil Engineering, The University of Queensland, Brisbane, Australia, p. 72.
[14] J. Chen, C. Liu, C. Zhang, H.J. Walker, Geomorphological development and sedimentation in Qiantang Estuary and Hangzhou bay, J. Coastal Res. 6 (3) (1990) 559–572.
[15] B. Tessier, J.H.J. Terwindt, 1994, An example of soft-sediment deformations in an intertidal environment—the effect of a tidal bore, Compt.-Rend. Acad. Sci. Sér. II, Part 2, 319(2) 217–233, (in French).
[16] S.F. Greb, A.W. Archer, Soft-sediment deformation produced by tides in a Meizoseismic area, Turnagain Arm, Alaska, Geology 35 (5) (2007) 435–438.
[17] H. Chanson, M. Trevethan, C. Koch, Turbulence measurements with acoustic doppler velocimeters, J. Hydraul. Eng. ASCE 133 (11) (2007) 1283–1286. doi:10.1061/(ASCE)0733-9429(2005)131:12(1062).
[18] N.J. Docherty, H. Chanson, 2010, Characterisation of unsteady turbulence in breaking tidal bores including the effects of bed roughness, Hydraulic Model Report No. CH76/10, School of Civil Engineering, The University of Queensland, Brisbane, Australia, p. 112.
[19] D.G. Goring, V.I. Nikora, 2002, Despiking acoustic Doppler velocimeter data, J. Hyd. Engrg., ASCE, 128(1) 117–126; 129(6) 484–489 (discussion).
[20] P. Bradshaw, An introduction to turbulence and its measurement, in: The Commonwealth and International Library of Science and Technology Engineering and Liberal Studies, Thermodynamics and Fluid Mechanics Division, Pergamon Press, Oxford, UK, 1971, p. 218.
[21] J. Piquet, Turbulent Flows. Models and Physics, Springer, Berlin, Germany, 1999, p. 761.
[22] R. Michel, J. Cousteix, R. Houdeville, Unsteady Turbulent Shear Flows, Springer Verlag, Berlin, Germany, 1981, p. 424.
[23] B. Stutz, J.L. Reboud, Experiments in unsteady cavitation, Exp. Fluids 22 (1997) 191–198.
[24] J.H. Trowbridge, On a technique for measurement of turbulent shear stress in the presence of surface waves, J. Atmos. Ocean. Technol. 15 (1998) 290–298.
[25] W.J. Shaw, J.H. Trowbridge, The direct estimation of near-bottom turbulent fluxes in the presence of energetic wave motions, J. Atmos. Ocean. Technol. 18 (2001) 1540–1557.
[26] H. Chanson, D. Reungoat, B. Simon, P. Lubin, 2011, High-frequency turbulence and suspended sediment concentration measurements in the Garonne river tidal bore, Estuarine Coastal Shelf Sci. Online First.
[27] H. Favre, 1935, Etude théorique et expérimentale des ondes de translation dans les canaux découverts, Theoretical and Experimental Study of Travelling Surges in Open Channels, Dunod, Paris, France (in French).
[28] A. Treske, 1994, Undular bores (Favre-Waves) in open channels—experimental studies, J. Hyd. Res., IAHR, 32(3) 355–370; 33(3) 274–278 (discussion).
[29] J.S. Montes, Hydraulics of Open Channel Flow, ASCE Press, New York, USA, 1998, p. 697.
[30] F. Benet, J.A. Cunge, Analysis of experiments on secondary undulations caused by Surge waves in trapezoidal channels, J. Hyd. Res. IAHR 9 (1) (1971) 11–33.
[31] P. Navarre, 1995, Aspects physiques du caracteres ondulatoire du macaret en Dordogne, Physical Features of the Undulations of the Dordogne River Tidal Bore D.E.A. thesis, Univ. of Bordeaux, France, p. 72 (in French).